

Instrument Science Report WFC3 2009-46

WFC3 SMOV Programs 11425, 11435: IR Channel On-orbit Alignment

G. Hartig, L. Dressel, and T. Delker
14 December 2009

ABSTRACT

Following the insertion of WFC3 into the HST observatory during Servicing Mission 4, we aligned the UVIS and IR channels, independently, to the telescope early in the SMOV4 instrument verification campaign. Using a variety of techniques, and accounting for the OTA temporal focus variation, we adjusted the instrument corrector mechanisms to optimize image quality. The IR channel alignment observations, analysis techniques and resulting adjustments are described herein; alignment of the UVIS channel is treated in a separate report.

Introduction

Each of the HST science instruments (SIs) installed in the observatory on-orbit during servicing missions must be aligned to the telescope. Although WFC3 was shown to be well-aligned to its nominal optical telescope assembly (OTA) interface, as represented by the ground support test hardware during pre-launch testing (Hartig, 2008), the instrument latch position uncertainties and the effects of gravity release, in particular, are sufficiently large that the stringent requirements for pupil alignment and focus cannot be met with ground testing and adjustment alone. The image quality is particularly sensitive to registration of the OTA exit pupil with the SI entrance pupil, since the SI must correct the large spherical aberration produced by the OTA. Pupil shear of less than 1% results in noticeable coma. Hence the SIs generally incorporate corrector mechanisms to permit accurate pupil alignment as well as to adjust focus. (An exception is the Cosmic Origins Spectrograph, for which pupil alignment is achieved by repointing the observatory and repositioning its aperture.)

The corrector mechanisms used in both the IR and UVIS channels of the WFC3 are based on the design employed by the ACS, which consists of a nested eccentric cylinder pair (“Wally Wobbler”) to effect tip and tilt of the mirror which serves to image the OTA pupil on the corrective optic, riding on a linear focus stage, all driven by redundantly-wound stepper motors. Resolvers provide absolute position feedback for the cylinders, while linear variable differential transducers (LVDTs) indicate the focus position; these positions are

downlinked in the engineering telemetry stream and included in the support (.spt) files produced by the OPUS pipeline. Because the optical beam is folded at the mirror on the corrector mechanism, linear motion of the focus stage also produces some pupil shear, which must be accounted for in optical performance analyses. This coupling is particularly severe for the IR channel, as discussed by Hartig (2005).

Focus adjustment, while inherently straightforward, is complicated by the temporal variation of the OTA focus (“breathing”) caused by thermally-induced changes in the telescope structure. While this effect has been modeled using data from the OTA thermal sensors, the model does not accurately predict the absolute focus over the long term, but can be effectively used to improve relative focus assessment through a single orbit. Final focus adjustment must therefore be based on the ensemble of focus measurements obtained through the alignment process.

This report details the on-orbit alignment process, describing the observations and analysis techniques used to rapidly converge on the near-optimal alignment of the IR channel. The UVIS channel alignment is similarly treated in a companion report (Hartig, et al. 2009). A chronology of the measurements and a log of the corrector mechanism adjustments are presented. Final confirmation of the IR imaging performance is described elsewhere (Hartig, 2009).

Observations

The alignment program proceeded in two stages, beginning with relatively coarse, five position focus sweeps in 250 step increments from -500 to +500 steps from the current nominal position. These produce image sets with sufficient focus diversity (± 0.48 mm at the detector, corresponding to 126 nm RMS focus or $\lambda/8$ at 1 μ) which permits reasonably accurate phase retrieval (PR) assessment of the wavefront error (WFE), especially coma, from which pupil alignment corrections can be determined. While greater focus range would yield greater WFE measurement accuracy, motion of the focus stage was limited due to thermal concerns (the motor temperature rises rapidly during actuation) and the desire not to move to positions too far from best focus, at which severe impact to the scientific capability of the instrument would result in the very unlikely event of stage failure.

These focus scans were implemented with SMOV4 program 11425, which specified three visits, separated by at least 48 hrs., to permit data acquisition, analysis and uplink of the required corrections before the next observation set was obtained. All of the observations are specified with relative focus and cylinder motor step offsets. Each visit may result in adjustments to the corrector mechanism inner or outer cylinder rotational positions, to improve pupil alignment, and/or focus stage position. The adjustments are effected by real-time commands of relative motor step offsets, specified in Operations Requests to the STOCC at GSFC and generally routed through the STScI SI commanding group. The IR detector was operated at its nominal temperature, -128 C, and nominal gain (2.5 e⁻/DN), and all images were obtained with the full field format, with 15 readout samples in RAPID mode to improve dynamic range and permit cosmic ray rejection.

The WFC3 pupil misalignment with respect to the OTA indicated by these measurements was larger than expected, amounting to ~ 3 arcminutes, as deduced by the required cylinder

adjustments and change in boresight, on both UVIS and IR channels, which deviated in similar magnitude and direction. While the consequence for the UVIS channel is negligible, the IR corrector cylinders required offsets to a region not in our experience base. Since the orientation of the angular offset from each cylinder depends on its absolute position (and is not orthogonal between inner and outer cylinders), we had to rely on a model produced by one of us (T.D.), anchored with mechanism level test data obtained at Ball Aerospace, to compute the corrective offsets. This was later improved using the cylinder raster data from the fine alignment program (11435).

After the alignment was nearly optimized, a fine 9-position focus scan, using 125-step increments, was executed with program 11435, followed by a 9 point tip/tilt raster, with ± 12 step offsets of each cylinder from its current position, to assure that the pupil alignment had been achieved. These offsets correspond to ~ 12 nm RMS coma, while the design residuals vary by about ± 10 nm RMS over the field. It is best that the focus be set before making the final adjustment of the tip/tilt (pupil) alignment because of potential wobble in the linear focus stage, which can produce unpredictable pupil shear as focus is adjusted.

The target for both programs is a field in NGC-188, an astrometric old open cluster, chosen to yield a reasonable density of appropriately bright stars to permit accurate encircled energy measurements while sampling the FOV well with relatively short exposures in the F127M filter used for all of these alignment images. The moderate bandpass and central wavelength of this filter permit accurate PR analysis to determine the WFE. The high latitude of NGC-188 makes it available year-round, and, if guide stars are selected from the astrometric catalog (ID=ZZZZ), then absolute boresight measurements are also possible. The chosen field is centered on the star designated #58 in the astrometric catalog; this star turns out to be binary, so is not particularly useful in itself for either astrometric or imaging performance evaluations, but there are many stars in the field that do support both analyses.

Logs of the observations for all visits of both programs are listed in Appendix A. These include the absolute corrector mechanism positions for each exposure, indicated as triads of focus stage LVDT, and inner and outer cylinder resolver readbacks, in that order. The modeled OTA breathing (brth) is also listed, in microns of secondary mirror (SM) despace.

Analyses

The NGC-188 field images were analyzed by first identifying suitable stars, which are of sufficient signal level (>3 - 5 kDN in the peak px), and isolated from neighbors and field edges, bad pixels, etc. in order to permit accurate encircled energy computation. This selection was accomplished with IDL tool *findstars*, which, after automatically selecting suitable PSFs, permits manual inspection of the results, enabling further vetting. About 20 stars, distributed over the field, were typically selected this way for analysis. Figure 1 displays the field with selected stars identified from program 11425 visit 3.

The focus scan measurements were made using idl tool *fscan_smov*, which computes the encircled energy (EE) in a 0.35 arcsec diameter for each of the selected stars at each focus position, excludes outliers, and plots the EE averaged over the field vs. focus. The OTA

breathing model was used to estimate the telescope focus state at the time of each observation and correct the nominal focus positions. A parabola was then fit to the data to determine the optimal focus setting. Figure 2 shows the results of the program 11425 visit 3 scan. The error bars represent the standard deviation of the measurements over field for each focus setting.

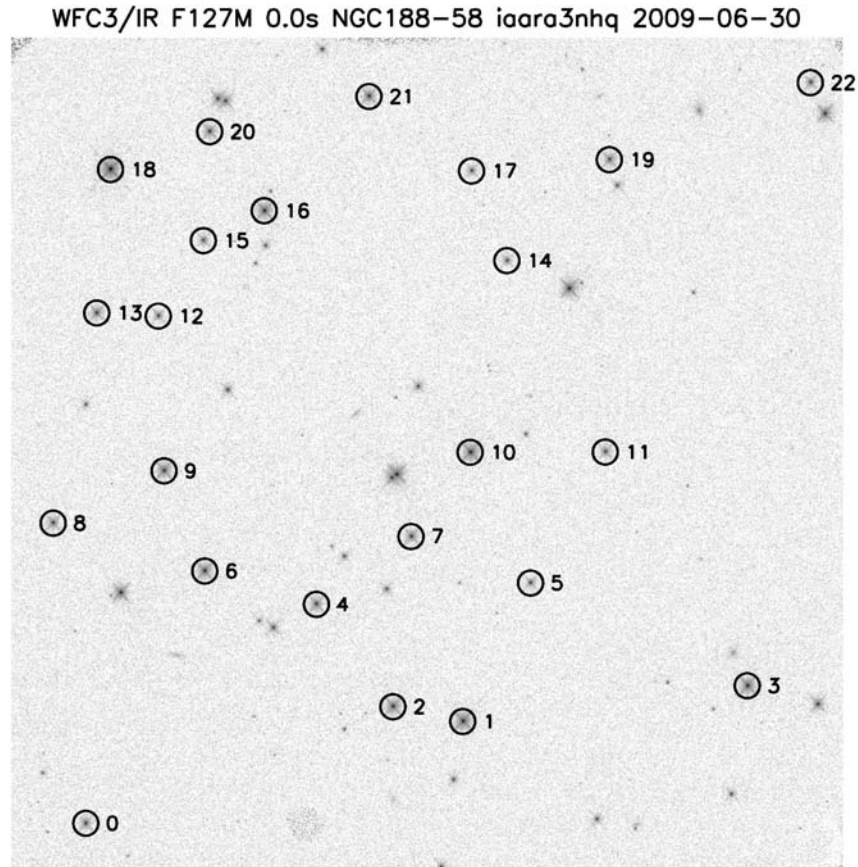


Figure 1. The NGC 188 field showing stars selected for analysis from visit 3 of program 11425.

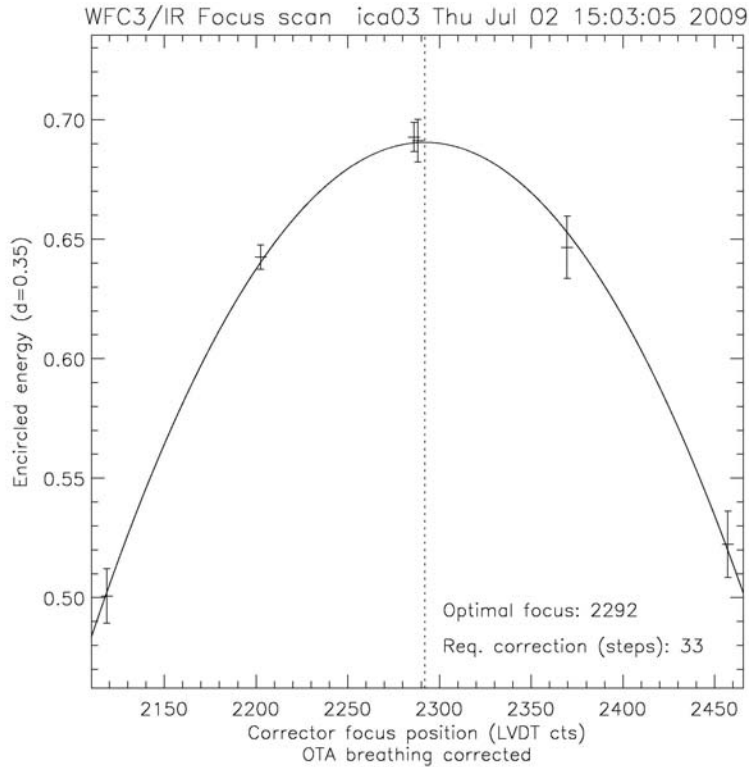


Figure 2. Encircled energy vs focus position for visit 3 of program 11425.

The pupil alignment is evaluated with IDL tool *align_smov*, which uses *wfc3fitc* to perform PR analysis to determine the low-order WFE for each star, simultaneously fitting images from the 5 focus positions. The WFE data are then used to compute the corrector cylinder offsets required to compensate the measured coma using sensitivity factors and coordinate transformations determined empirically or by modeling (and confirmed by measurement), as encoded in *wfc3_ir_corr*. Figure 3 shows the resultant map of cylinder step corrections for each field point and the mean over all of the measured points, which was adopted as the desired offset to be applied. The scatter in the results represents the intrinsic field-dependent design residual and internal alignment errors as well as the measurement uncertainty, which varies from star to star depending on the signal level, presence of uncorrected detector artifacts, such as hot pixels, and CRs, etc.

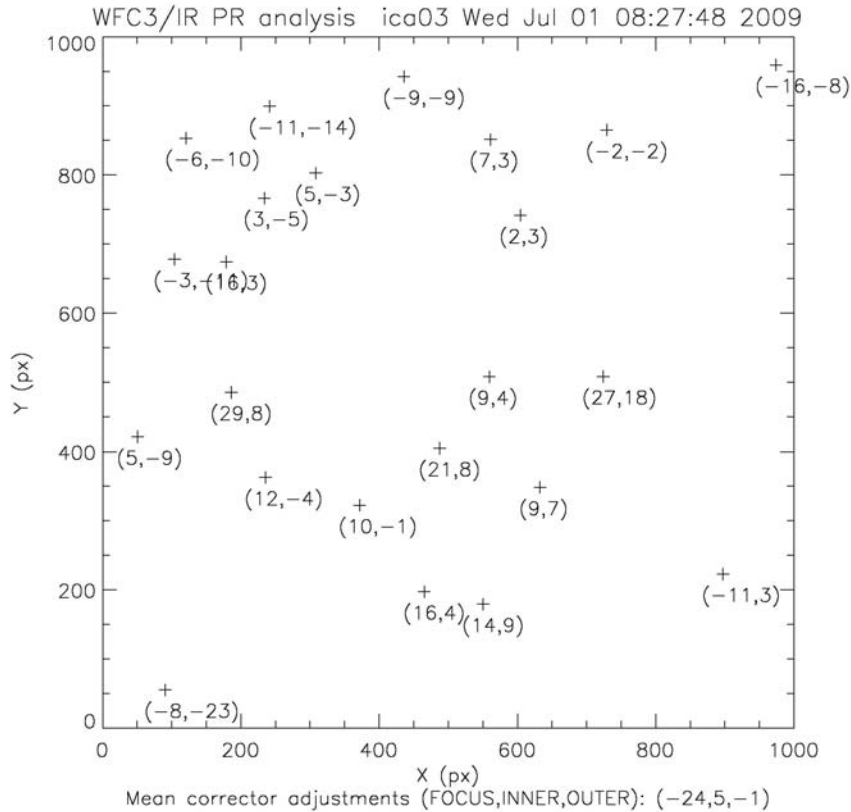


Figure 3. PR results for visit 3 of program 11425 showing the corrector cylinder offsets required to minimize coma at each field point.

As mentioned above, the use of the corrector focus stage to provide focus-diverse image sets for PR analysis may result in unpredictable amounts of pupil shear (and resulting coma) due to wobble of the mirror on the stage. This was ameliorated by using the measured image location offsets to estimate the mechanism-induced coma contribution and add it to the WFE estimate at each focus position during the iterative fit process in *wfc3fitc*.

The program 11435 tip/tilt raster images were analyzed using both EE and PR techniques on each image. The resultant coma estimates were plotted against relative inner and outer cylinder step position, with contours fit to visualize the coma distribution. Because there is no focus diversity in these PR analyses (single images near optimal focus were fit), the accuracy is poor relative to that obtained with the focus scan data. The EE measurements were also plotted in the same manner. These results are depicted in Figure 4 for the visit 2 fine alignment observation, and indicate that optimal pupil alignment is displaced somewhat from that determined in the coarse alignment phase. Both EE and PR results favor an inner cylinder correction of ~ -9 steps, and a smaller negative correction for the outer cylinder. We adopted the EE results as being more trustworthy and indicative of the true optical performance and requested a final adjustment of -3 steps on the outer cylinder.

The final, fine focus scan data were treated in the same fashion as the coarse scans described above. Because the OTA long term focus was determined to have drifted over the past several years to be sufficiently long of the common position optimal for the pre-SM4 instruments (ACS, STIS, NICMOS), an adjustment of the OTA SM despace by $+3 \mu$ was planned for 20 July 2009. The optimal adjustment was estimated at 2.5μ and an additional

0.5 μ was added to overcompensate since continued focus drift is expected. The final WFC3 focus setting anticipated this OTA focus adjustment and included a +63 step offset to compensate the 2.5 μ SM shift in addition to the +30 step offset deduced from the ensemble of focus scans to date.

Table 1 lists each of the corrector adjustments made throughout the SMOV4 alignment program to achieve near-optimal optical performance. The net adjustments indicate that the instrument was originally positioned in the HST observatory within ~ 0.4 mm of optimal focus and ~ 3 arcminutes of the desired chief ray angle.

Table 1. WFC3/IR Corrector Adjustment Log

date	prop:visit	Focus		Inner Cylinder		Outer Cylinder	
		Δ steps	LVDT	Δ steps	resol	Δ steps	resol
24-Jun	First Light		2279		54192		43069
26-Jun	11425:1	0	2279	-50	51150	-80	38216
28-Jun	11425:2	0	2279	34	53119	30	40033
30-Jun	11425:3	0	2279	5	53436	0	40033
2-Jul	11435:1	93	2305	-5	53145	-3	39853
5-Jul	11435:2	0	2305	-9	52714	-3	39670
9-Jul	11435:4	0	2305	0	52714	0	39670
Net adjustment:		93		-25		-56	

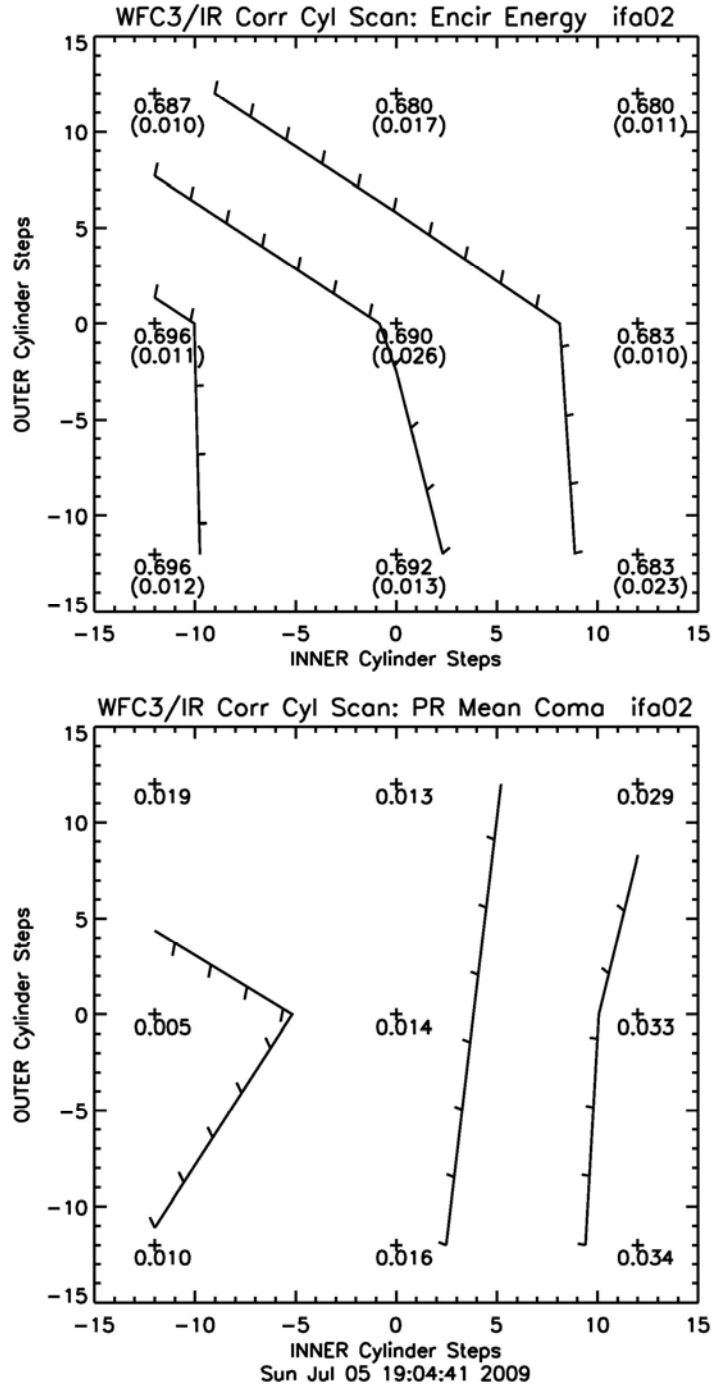


Figure 4. EE and PR results for the corrector cylinder raster scan of visit 4 of program 11435.

Conclusion

The WFC3 IR channel was successfully aligned on-orbit during the scheduled SMOV4 program. Although the initial misalignment required corrections that used the corrector mechanism cylinders beyond our experience range, final alignment was achieved on 7 July 2009, with uplink of the last small adjustments. Because the focus, determined with only a few observations, is somewhat uncertain due to the OTA breathing, continued monitoring of the image quality at a larger variety of breathing states may indicate that further adjustment is warranted. If this is attempted, a cylinder scan should be scheduled after the focus adjustment to enable compensation for any pupil shear that may occur as a result.

Acknowledgements

The authors are grateful to Matt Lallo, Colin Cox and Chris Long for assistance in determining the OTA focus state and providing the breathing model data, which were essential to setting the WFC3 focus.

References

Hartig, G.F. "WFC3 IR Channel Corrector Alignment", STScI ISR WFC3-2005-03, 2005

Hartig, G.F. "WFC3 Optical Alignment Characterization in Thermal-Vacuum Test #3", STScI ISR WFC3-2008-32, 2008

Hartig, G.F. "WFC3 SMOV Proposals 11437/9: IR On-orbit PSF Evaluation", STScI ISR WFC3-2009-37, 2009

Hartig, G., Dressel, L., and Delker, T. "WFC3 SMOV Proposals 11434/6: UVIS Channel On-orbit Alignment", STScI ISR WFC3-2009-45, 2009

Appendix A. Observation Logs

11425\visit1

rootname	obs_date	obs_time	exptime	brth	corrector_pos
iaar01onq	09-06-26	15:46:29	43.98	0.9	(2300,54192,43069)
iaar01ooq	09-06-26	15:49:10	43.98	1.0	(2115,54192,43069)
iaar01orq	09-06-26	16:41:21	43.98	-0.2	(2200,54192,43069)
iaar01osq	09-06-26	16:44:02	43.98	0.0	(2365,54192,43069)
iaar01ouq	09-06-26	16:57:30	43.98	0.4	(2454,54192,43069)
iaar01ovq	09-06-26	17:00:11	43.98	0.3	(2284,54192,43069)

11425\visit2

rootname	obs_date	obs_time	exptime	brth	corrector_pos
iaara2zsq	09-06-28	17:59:20	43.98	-0.5	(2284,51150,38216)
iaara2ztq	09-06-28	18:02:01	43.98	-0.5	(2113,51150,38216)
iaara2zvq	09-06-28	18:15:29	43.98	-0.0	(2198,51150,38216)
iaara2zwq	09-06-28	18:18:10	43.98	-0.1	(2364,51150,38216)
iaara2zyq	09-06-28	18:31:38	43.98	0.3	(2452,51150,38216)
iaara2zzq	09-06-28	18:34:19	43.98	0.6	(2283,51150,38216)

11425\visit3

rootname	obs_date	obs_time	exptime	brth	corrector_pos
iaara3nhq	09-06-30	22:37:57	43.98	-0.9	(2281,53119,40033)
iaara3niq	09-06-30	22:40:38	43.98	-0.9	(2111,53119,40033)
iaara3nkq	09-06-30	22:54:06	43.98	-0.9	(2195,53119,40033)
iaara3nlq	09-06-30	22:56:47	43.98	-0.9	(2362,53119,40033)
iaara3nnq	09-06-30	23:10:15	43.98	-0.9	(2450,53119,40033)
iaara3noq	09-06-30	23:12:56	43.98	-0.7	(2280,53119,40033)

11435\visit1

rootname	obs_date	obs_time	exptime	brth	corrector_pos
iaav01t8q	09-07-03	00:04:41	43.98	1.1	(2280,53436,40033)
iaav01t9q	09-07-03	00:07:22	43.98	1.1	(2110,53436,40033)
iaav01tbq	09-07-03	00:20:50	43.98	1.0	(2149,53436,40033)
iaav01tcq	09-07-03	00:23:31	43.98	1.0	(2194,53436,40033)
iaav01teq	09-07-03	00:36:59	43.98	1.0	(2238,53436,40033)
iaav01tfq	09-07-03	00:39:40	43.98	1.0	(2278,53436,40033)
iaav01thq	09-07-03	00:53:08	43.98	1.0	(2318,53436,40033)
iaav01tiq	09-07-03	00:55:49	43.98	1.0	(2360,53436,40033)
iaav01tkq	09-07-03	01:49:37	43.98	0.8	(2405,53436,40033)
iaav01tlq	09-07-03	01:52:18	43.98	0.8	(2448,53436,40033)
iaav01tnq	09-07-03	02:05:46	43.98	0.8	(2279,53436,40033)

11435\visit2

rootname	obs_date	obs_time	exptime	brth	corrector_pos
iaava2nhq	09-07-05	13:04:55	43.98	-2.3	(2307,53128,39853)
iaava2niq	09-07-05	13:07:36	43.98	-2.3	(2307,52396,39127)
iaava2nkq	09-07-05	13:21:04	43.98	-1.9	(2308,52396,39853)
iaava2nlq	09-07-05	13:23:45	43.98	-1.8	(2307,52396,40582)
iaava2nuq	09-07-05	14:18:26	43.98	-1.0	(2307,53114,39126)
iaava2nvq	09-07-05	14:21:07	43.98	-1.3	(2307,53114,39853)
iaava2nyq	09-07-05	14:34:35	43.98	-3.1	(2307,53114,40581)
iaava2nzq	09-07-05	14:37:16	43.98	-3.0	(2307,53831,39126)
iaava2olq	09-07-05	14:50:44	43.98	-2.4	(2307,53831,39854)
iaava2o2q	09-07-05	14:53:25	43.98	-2.6	(2308,53831,40582)
iaava2otq	09-07-05	15:06:53	43.98	-1.8	(2307,53145,39853)

11435\visit4

rootname	obs_date	obs_time	exptime	brth	corrector_pos
iaav04agq	09-07-09	23:41:32	43.98	0.6	(2308,52714,39670)
iaav04ahq	09-07-09	23:44:13	43.98	0.4	(2136,52714,39670)
iaav04ajq	09-07-09	23:57:41	43.98	-1.6	(2179,52714,39670)
iaav04akq	09-07-10	00:00:22	43.98	-1.8	(2225,52714,39670)
iaav04amq	09-07-10	00:13:50	43.98	-1.9	(2265,52714,39670)
iaav04anq	09-07-10	00:16:31	43.98	-1.8	(2304,52714,39670)
iaav04apq	09-07-10	00:29:59	43.98	-0.7	(2346,52714,39670)
iaav04aqq	09-07-10	01:17:46	43.98	0.5	(2391,52714,39670)
iaav04asq	09-07-10	01:31:14	43.98	-1.7	(2435,52714,39670)
iaav04atq	09-07-10	01:33:55	43.98	-1.8	(2475,52714,39670)
iaav04avq	09-07-10	01:47:23	43.98	-2.3	(2305,52714,39670)